Fermi National Accelerator Laboratory

FERMILAB-Pub-86/105-E
7000.740

ACCURATE 2 DIMENSIONAL DRIFT TUBE READOUT USING TIME DIVISION AND VERNIER PADS*

D. Green, H. Haggerty, S. Hansen, and M. Takasaki
Fermi National Accelerator Laboratory, Batavia, IL 60510 USA

July 1986

*Submitted to Nuclear Instruments and Methods A

ACCURATE 2 DIMENSIONAL DRIFT TUBE READOUT USING TIME DIVISION AND VERNIER PADS

D. Green, H. Haggerty, S. Hansen, M. Takasaki

Fermi National Accelerator Laboratory

Batavia, Illinois 60510

ABSTRACT

A proportional drift tube (PDT) of length ℓ = 6m containing only two potentials for a 5cm drift distance has been constructed. The coordinate along the drift direction is obtained conventionally. The second coordinate is obtained with an accuracy of $\pm$ 0.8mm (r.m.s.) by utiizing a combination of time division[1] and vernier pads[2], of length L = 20 cm. The left/right drift time ambiguity can be resolved using separate top and bottom vernier pad readout.

INTRODUCTION

The problem of covering a large surface area with accurate position measuring devices is largely economic. For collider experiments such as DØ[3], the cost of material for muon coverage scales as the surface area of the chambers. This cost is non-negligible. In addition, crossed plane ambiguities are always annoying. Hence, 2 dimensional readout of the cells has been chosen. The coordinate in one direction is obtained quite accurately by conventional drift time measurements. The electrostatics which was chosen saturates the drift velocity in the gas over the 1 μsec maximum drift time allowed by the DØ trigger requirements[3].

The choice of Ar-C_2H_6 (1:1) as the PDT gas means that[4] a field of $\geq$ 500 Volt/cm throughout the drift cell will maintain the drift velocity within 5% of its saturated value of v_d=53.8 mm/μsec=[18.6 nsec/mm]$^{-1}$. The total drift time for a maximum 5 cm drift distance is 930 nsec. The required fields are obtained by a field shaping electrode run at +3.0 kV and the a=25 μm radius gold clad tungsten wire run at +5.6 kV. The equipotentials and equal time contours are shown in Figures 1a and 1b respectively, for the electrode dimensions chosen.

The contours of Fig. 1b are evenly spaced in the Z=0 plane, indicating that the desired saturation has been reached. Shown in Fig. 2 are the measured drift times as a function of y using cosmic rays and external drift chambers to measure y. Since drift velocity saturation has been achieved, the chambers will be insensitive to gas temperature and pressure variations[4].

The measurement of the drift coordinate will be ultimately limited by diffusion[5]. For this gas[4], the limit is σ_D=100 $\mu m\sqrt{y(cm)}$, or σ_D=224 μm or σ_D/v_d= 4.2 nsec[6]. An accurate measurement of the drift time and the prior existence of an extra electrode invite a measurement of the second orthogonal coordinate using a combination of time division (coarse) and vernier pads (fine). A major advantage of time division over charge division is that the front end electronics for time division already exists in the drift time measurement hardware. The pad shapes, padsizes(ℓ and L), the coordinate (x), and the signals (Q_1, Q_2, Q_3, Q_4, t_A, t_B) for a prototype PDT are all defined in Figure 3a. This prototype used long pads, of size ℓ, for an initial study. The final PDT for the DØ muon detector will rely solely on short pads and use only Q_1, Q_2, t_A, and t_B. The angles subtended by the pads as viewed by the wire are defined in Figure 3b. A thorough analysis of the time division technique is available in Ref. 1.

PDT PARAMETERS

The PDT shown in Figure 1 has a set of intrinsic source parameters which define the ultimate accuracy of the position measurement. For ease of access to the electronics the PDTs are serviced at one end only[3]. Adjacent PDT wires are tied together as indicated in Figure 3a. Then t_A=x/c, t_B=(2ℓ-x)/c and Δt=t_B-t_A=2(ℓ-x)/c, where c is the speed of light. Hence the resolution on Δt is $d(\Delta t)=\sqrt{2}\,dt_A = 2\,dx/c$.

Operating at a wire voltage of V_o = 2600 V with respect to the pads in $Ar-C_2H_6$ (1:1) yields a gas gain of ~ 1.8 x 10^5 or ~ 3.2 pC of charge (Q) on the a=25 μm radius wire. The electric field at the wire surface is 160 kV/cm. The charge Q has been measured by measuring $Q_s=Q_1 + Q_2$ which is the total charge on the pads. The charge distribution for cosmic ray events is shown in Figure 4. The mean is roughly $\bar{Q}_s$ = 1.6 pC, which implies a wire charge Q whose mean is about 3.2 pC.

The ion mobility of argon is μ^+ = 1.5 $cm^2 sec^{-1} V^{-1}$.[4] The characteristic pulse formation time[7] is $t_o=a^2 \ell n(b/a)/(2\mu^+ V_o)$= 5.5 nsec; a is the wire radius and b is the field shaping electrode radius (b ~ f, see Fig. 1a). For low input impedance amplifiers, the charge Q is delivered as a current pulse i(t).

$$i(t) = \frac{Q}{2\ell n(b/a)t_o}\left[\frac{1}{1+t/t_o}\right] \qquad (1)$$

For Q=3.2 pC of delivered charge, i(o)=42 μA.

For analysis purposes the tube shown in Fig. 1 can be considered to be a co-axial cylinder of outer radius b ~ 2.5 cm. Treating the PDT as a wave guide, the capacity/length is $C=2\pi\varepsilon_o/\ell n(b/a)$=8.1 pf/m. The characteristic impedance is $Z_o=1/2\pi\sqrt{\mu o/\varepsilon o}\ \ell n(b/a)$ ~ 414 Ω.

However, the wave guide is not lossless. At frequencies <100 MHz, the skin depth in tungsten is > 12 μm. The gold cladding is too thin to be a factor. This means that there are losses due to the resistance $R=\rho\ell/\pi a^2$ where ρ is the conductivity. For ℓ=6 m, R is 165 Ω. The characteristic rise time for the line is then $\tau=RC\ell=\rho\ell^2 C/\pi a^2$=8.2 nsec. This finite resistance and finite rise time are the basic limitations to the accuracy of the position measurement for this tube.

FRONT END PARAMETERS

A simplified schematic of the time to voltage conversion electronics (TVC) is shown in Figure 5. The pulses t_A and t_B (defined in Figure 3) are amplified and discriminated with threshold current i_T. The time difference $\Delta t = t_B - t_A$ is converted into a voltage by charging a capacitor C with current source I for time Δt. The delay is equal to $(2\ell/c)$ and insures that "set" always proceeds "reset" for the flip flop.

A more detailed schematic of the front end amplifier and discriminator is shown in Figure 6. The 330 Ω termination resistor plus r_E (~ 250 Ω at I_E ~ 0.1 mA) roughly matches Z_o. The common base bias is chosen for high speed operation. The ft value of the BFS17 transistor at I_E=0.1 mA exceeds that of the μA733 amplifier.

The thermal noise current due to the termination resistor R_T is $(i'_n)_T^2 = 4kT/R_T$ or $(i'_n)_T \sim 7$ pA/$\sqrt{HZ}$. There is also comparable noise due to the $2R = 330\Omega$ resistance of a 2ℓ length of anode wire as seen in Figure 5. The shot noise due to the standing bias current is $(i'_n)_s^2 = e\ I_E$ or $(i'_n)_s = 4$ pA/$\sqrt{HZ}$. A rough preamp noise estimate is $(i'_n) = 10$ pA/$\sqrt{HZ}$.

The μA733 amplifier has an ft value of 120 MHZ. The gain is 100 x at high frequencies and is clipped to 10 x at low frequencies. This clipping means that there is a minimum 2 hit resolution of T ~ 50 nsec. The time T corresponds to the resolution (with 2 hit electronics) of δ rays and muons with separation in the drift direction greater than 2.5 mm. Even though 2 adjacent tubes are connected together, 2 hits can be assigned correctly to their respective tubes because there exists a "time checksum" for valid pairings, $t_A + t_B = 2\ell/c$. The μA733 pulse response has a rise time less than the intrinsic tube rise time τ, and is thus adequate. Finally the LM360 slew is <3 nsec for 2x to 20x overdrive.

The noise source at the input, with a shaping of 50 nsec = T is $i_n \sim i'_n(\sqrt{T})^{-1} \sim$ 0.045 μA. The measured value for V_T corresponds to different i(o) thresholds. It is (100 mV/μA) x 10 for pulse injection at the BFS17, (50 mV/μA)x 10 at the far end of the tube due to the 2ℓ of loss (165Ωx2/(165x2+414)=0.44).

NOISE AND TIME RESOLUTION

The detailed schematic of the higher level 2 hit TVC electronics is shown in Figure 7. The analog outputs are sampled by a 13 bit scanning ADC. The observed rms resolution when t_A and t_B are pulsed simultaneously and the PDT is disconnected is d(Δt)= ±70 psec in Δt, or dt= ±50 psec in t, or dx= ±1 cm in intrinsic electronics resolution at large source impedance. Hence, the electronics is not the limitation, but rather the source itself.

Injecting a 12μA pulse into the PDT at x=0, (see Fig. 5, 6 μA into t_A, 6 μA into t_B) yields a mean and rms deviation of Δt as shown in Figure 8 for various threshold currents i_T. Noise limits i_T to be > 0.2 μA. The shift in the mean of Δt is due to tube losses which give a finite rise time τ. As defined in Figure 5, the dividers are $i_A = i(o)\ Z_o/2(Z_o+R_A)$, $i_B = i(o)\ Z_o/2(Z_o+R_B)$. These signals cross i_T at times, $t_A = (i_T/i_A)\tau_A$ and $t_B = (i_T/i_B)\tau_B$. Since $\tau_B \gg \tau_A$, $\Delta t \sim (i_T/i_B)\tau_B$. As seen in Fig. 8a, Δt is as predicted, proportional to i_T up to $i_T=i_B$ and varies roughly from zero to τ_B.

Since the signal rides on i_n and hence smears i_T by $di_T \sim i_n$, then at fixed i(0) the resolution in Δt due to i_n is

$$d(\Delta t) = \frac{2\, i_n}{i(0)} \left[\frac{Z_o+R_B}{Z_o}\right] \tau_B = (i_n/i_B)\ \tau_B \qquad (2)$$

This means that d(Δt) is expected to be independent of i_T which is seen to be approximately valid in Fig. 8b. The observed value of i_n is 0.05 μA, which is near

the estimate of 0.045 μA. Using Fig. 8a, one predicts that a noise i_n will smear Δt causing an error $d(\Delta t) = \pm 170$ psec, which agrees with Fig. 8b. The rms deviation of Δt is increased from ± 70 psec due to electronics ($\tau_B = 0$) to ±180 psec due to input noise.

Data were also taken with cosmic rays. The trigger was supplied by scintillation counters 1.5m long which covered seven of the short (L=20 cm) pads. The short pad charge ratio $(Q_2-Q_1)/(Q_2+Q_1)=\delta_L$ was used to accurately locate x modulo L (see Figure 3). The individual short pads are well resolved by the time division information, as seen in Fig. 9 which is a plot of Δt, projected using δ_L to the center of the pad. The resolution was observed to be $d(\Delta t)$=250 psec or dt=180 psec, or dx=±3.75 cm. At a mean position $\bar{x}=\ell/2$ the signal sees a series resistance R_A ~ 82Ω, R_B ~ 248Ω and has a risetime τ_A ~ 2.0 nsec, τ_B ~ 18.4 nsec. For these parameters equation (2) yields $d(\Delta t)=(0.1\ \mu A/42\ \mu A)\ ((414+248)/414)(18.4\ nsec)$ or $d(\Delta t)$~70 psec. This predicted resolution at a fixed i(0) corresponding to the mean Q_s shown in Fig. 4 is ~ 3.6 times smaller than the observed value. These data were taken with $i_T = 0.5$ μA. The variations in i(0) expected from Fig. 4 contribute to an additional time smearing $d(\Delta t)_Q$ identical to equation (2) but with i_n replaced by i_T, or $d(\Delta t)_Q$=350 psec. Saturation of the amplifier for i(0) > 75μA somewhat improves this expectation. Only a small shift in Δt correlated with the pad charge, $d(\Delta t)'_Q <$ 180 psec, was observed for the full excursion of Q. Hence, the pulse height corrections are less than the observed width. The data in Fig. 9 are not corrected for this variation.

Note that, at the crudest level, $d(\Delta t) = [2i_n/i(o)]\tau_B$. Ignoring logarithms the resolution scales as $i_n\rho\ell^2/Q$. The result obtained in Ref. 1 was dx=±0.85 cm for a ℓ=2m wire at a gas gain ~ 10^5. This result is consistent with our result, dx=±3.75cm, when scaled in this manner.

NOISE AND VERNIER PAD RESOLUTION

The basic electrostatics of the induced charge on pads is discussed elsewhere.[8] The geometry of the pads is shown in Figure 3. For a given wire charge Q, a pad charge is induced which depends on the solid angle subtended by the pads. The approximate result for an infinitely long strip is $Q_1 = Q(\theta_2-\theta_1)/\pi$, $Q_2 = Q\theta_1/\pi$ where $\tan\theta_1 = dx/2\ell f$ and $\tan\theta_2 = d/2f$. Then $Q_s = Q_1+Q_2 = Q\,[\tan^{-1}(d/2f)]/\pi$ which approaches Q/2 if $d>>f$. This result was used in Fig. 4 to relate the measured value of the pad source charge Q_s to the wire charge Q. The ratio of pad charges is used to measure x,

$$\delta_L = (Q_1 - Q_2)/(Q_1 + Q_2) = 1 - 2\theta_1/\theta_2. \qquad (3)$$

If $\tan\theta$ approaches θ then δ_L approaches $1 - 2x/L$ which is a linear relation of charge ratio to position. As is seen in what follows, the relationship for our geometry is only very roughly linear.

Having located which pad was hit by using time division, fine position information is obtained from the pad charges. A simplified schematic of the charge sensitive preamplifier (CSP) is shown in Figure 10a. With a pad width d=4.8 cm (see Fig. 3) and spacing the pad off ground by h=0.5 cm, there is a source capacity of C_s=275 pf for a ℓ=6 m pad. Baseline restoration is supplied by a conventional[9] dual baseline subtraction (BLS) for which a simplified schematic is shown in Figure 10b.

The source charge is $Q_s = Q/2 = 1.6$ pC. A detailed schematic of the CSP is shown in Fig. 11. The input FET has a noise voltage $e_n' \sim 1\text{nV}/\sqrt{\text{HZ}}$. With a BLS "before" minus "after" time (see Fig. 10) of ~ 1 μsec, set by triggering requirements, $e_n = e_n'\sqrt{f_{max}}$ ~ 1 μV. Driving the source capacity, there is then a noise charge of $Q_n = e_n C_s = 2.75 \times 10^{-4}$ pC. If only the input FET noise contributes there should be a signal/noise ratio of ~ 5800:1. We observe a pad pedestal rms of $dQ_1 = 1.5 \times 10^{-3}$ pC either with the PDT connected, or with a lumped capacitor = C_s connected to the CSP input. The

measured noise is then $dQ_1/Q_1 = 2dQ_1/Q_s = 1/533$ which indicates other sources of noise.

Cosmic ray test results for the PDTs built with ℓ=3.0 m and ℓ=6.0 m are shown in Figure 12a and Figure 12b respectively. The short pad (L=20 cm) ratio δ_L is used as an accurate probe of the long pad ratio, $\delta_\ell=(Q_4-Q_3)/(Q_4+Q_3)$. Hence the vertical axis is an accurate measure of x, while the intrinsic width of the curves is given by the poorer long pad measure of x. As in Fig. 9, seven short pads are illuminated and Fig. 12 is a picture of them as taken by the long pads, with distortions. Using equation (3), $d(\delta_L) \simeq 2dx/L$, so that for $Q_1=Q_2=Q_s/2$, $dx/L=(dQ_1/Q_1)/2\sqrt{2} \simeq 1/1510$. This is the expected resolution using the pedestal noise width.

Figure 12a implies that $dx/\ell = 0.0037 = 1/272$, while Figure 12b gives $dx/\ell \sim 0.0038 = 1/263$. These results do not scale in dx as ℓ as expected for noise dominated capacitive scaling by C_s. Since the observed Q_n is much larger than $e_n C_s$ this is not remarkable. The accuracy is also ~ 5 times worse than expected from the width of the pedestal. This means that the systematics and/or the extraneous noise sources are not yet fully understood. Note that production versions of the PDT will have symmetrically placed short pads above and below the anode wire (see Fig. 13a). This improved arrangement will be insensitive to misalignments of pads with respect to the wire in both y and z since the first derivatives of δ_L with respect to y and z vanish. In particular, the pads will be insensitive to wire sag. Even with the present systematic errors, the implied vernier pad resolution of $dx \sim \pm L/263 = \pm 0.76$ mm is more than adequate for most [3] purposes.

LEFT RIGHT DRIFT AMBIGUITY

The avalanche process itself is asymmetric[10]. In Figure 13a, is shown a pad configuration where top and bottom pads have the same shape, but are out of phase.

The resulting plot of δ_L^T vs δ_L^B which is shown in Figure 13b is double valued. The drifting ionization creates an avalanche which is to the left or the right of the wire. It is analogous to a wire misalignment which symmetric pads are designed to avoid. The large size of the effect is due to the long pad signal integration time. This effect could in fact be used to resolve the left right ambiguity. This fact has been checked by placing the trigger counters only on the left or only on the right and achieving a subsequent single valued δ_L^T versus δ_L^B plot.

If this effect were to be used then the number of layers of offset wires could be halved with the addition of two more analogue (pad) readout channels. This option would be economically preferable if the mechanical costs of the chambers exceeded the incremental electronics costs or if space were at a premium. One wire would then be able to provide the signed coordinate perpendicular to it (drift velocity with left/right ambiguity broken by top/bottom pads) and the coordinate along the wire (time division followed by charge ratio induced on the pads).

ACKNOWLEDGEMENTS

We would like to thank the other members of the DØ Muon Group for many suggestions and discussions. In particular, Dr. C. Brown performed the electrostatics calculations, and Dr. H. Jostlein and C. Lindenmeyer provided the parts for the mechanical construction of the test chamber. Dr. P. Martin first suggested to us the asymmetry in the avalanche process. We also thank the DØ Calorimetry Group for advice on analog electronics.

REFERENCES

1. R.A. Boie, V. Radeka, P. Rehak, and D.M. Xi
IEEE Trans. on Nuc. Sci., NS28, 471 (1981).

2. D.F. Anderson, et al., Nuc. Inst. Meth. in Phys. Res. 224, 315 (1984).

3. Design report, The DØ Experiment at the Fermilab Antiproton-Proton Collider, (1984).

4. A. Peisert and F., Sauli, CERN 84-08 (1984).

5. G. Charpak and F. Sauli, Ann. Rev. Nucl. Part. Sci. 34 285 (1984).

6. C. Brown et al., Fermilab TM-1301 (1985).

7. F. Sauli, CERN 77-09.

8. G. Fischer, J. Plch, Nuc. Inst. and Meth. 100 515 (1972).

9. T. Droege et al., IEEE Trans. on Nuc. Sci., NS25, 1 (1978).

10. G. Erskine, Nuc. Inst. and Meth. 198 325 (1982).

FIGURE CAPTIONS

1) Electrostatics for the proportional drift tubes.
   a) equipotential contours
   b) equal time drift contours
2) Drift time as a function of position y in the PDT.
3) a) Definition of lengths, pad charges and wire times for the test proportional drift tube.
   b) definition of the angles subtended by the pads.
4) Charge of the pads, $Q_1 + Q_2$ in pC as measured in cosmic ray triggered events.
5) Schematic of the time to voltage conversion circuit.
6) Detailed schematic of the TVC amplifier and discriminator.
7) Detailed schematic of the TVC flip flops, current sources, switches, and output buffers.
8) Test data on pulser response of the complete TVC system for various threshold currents i_T
   a) mean of time difference Δt
   b) rms width, $d(\Delta t)$ of time difference Δt.
9) Time difference response of the proportional tube for cosmic ray events. The time is slightly corrected by using the short pad ratio δ_L to put it at the center of each pad.
10) a) Schematic of the pad charge sensitive preamplifier (CSP).
    b) Schematic of the pad dual baseline subtracter (BLS).
11) Detailed schematic of the CSP circuit.

12) Cosmic ray test data. Short pad (L) ratio vs long pad (ℓ) ratio. Comparison of a) ℓ=3 m, b) ℓ=6 m test chambers.

13) a) Pad arrangement for symmetrized pads when $Q_1 = Q_1^T + Q_1^B$, $Q_2 = Q_2^T + Q_2^B$

b) δ_L^T vs δ_L^B when top and bottom pads are read out separately.

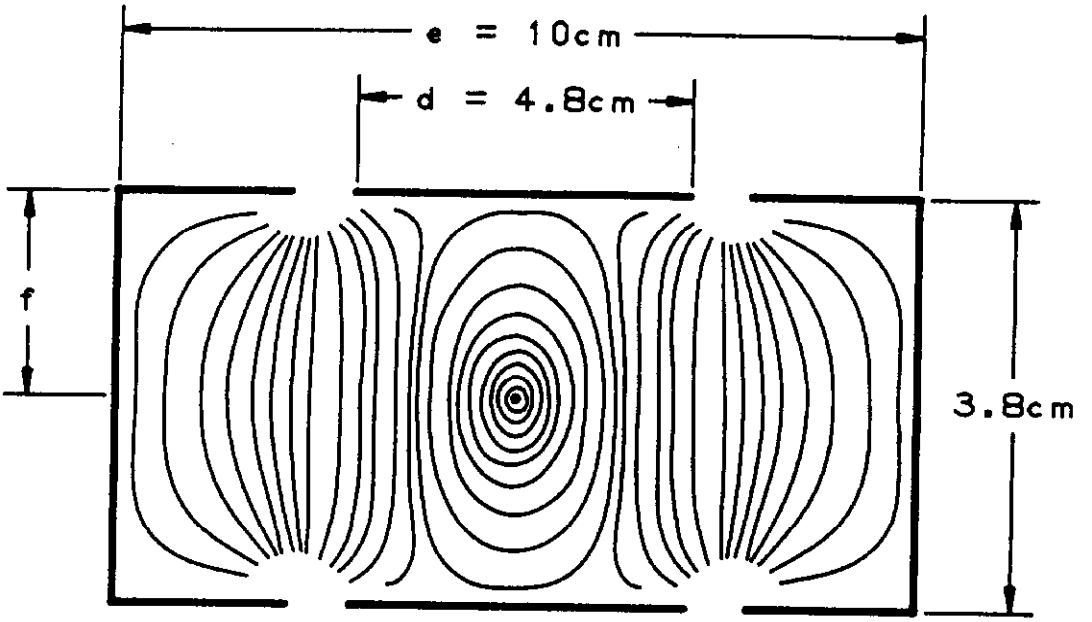

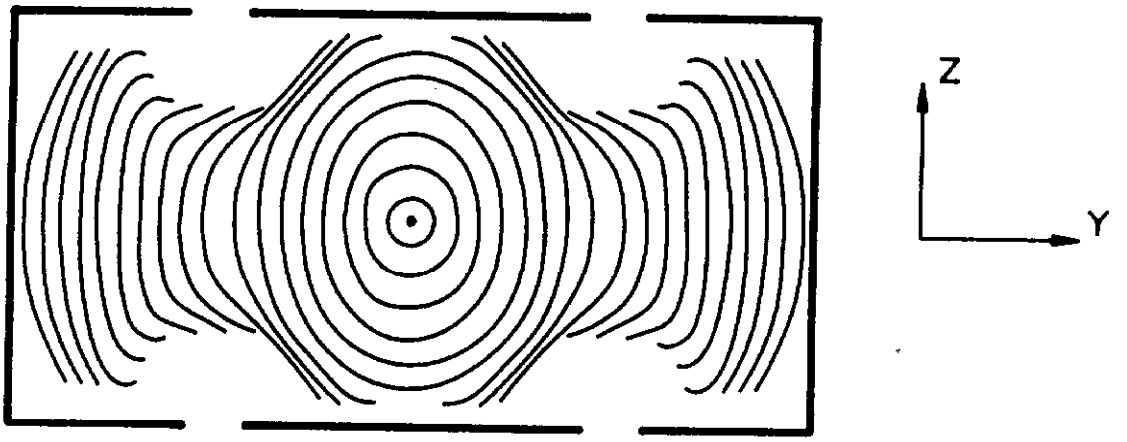

Fig. 1

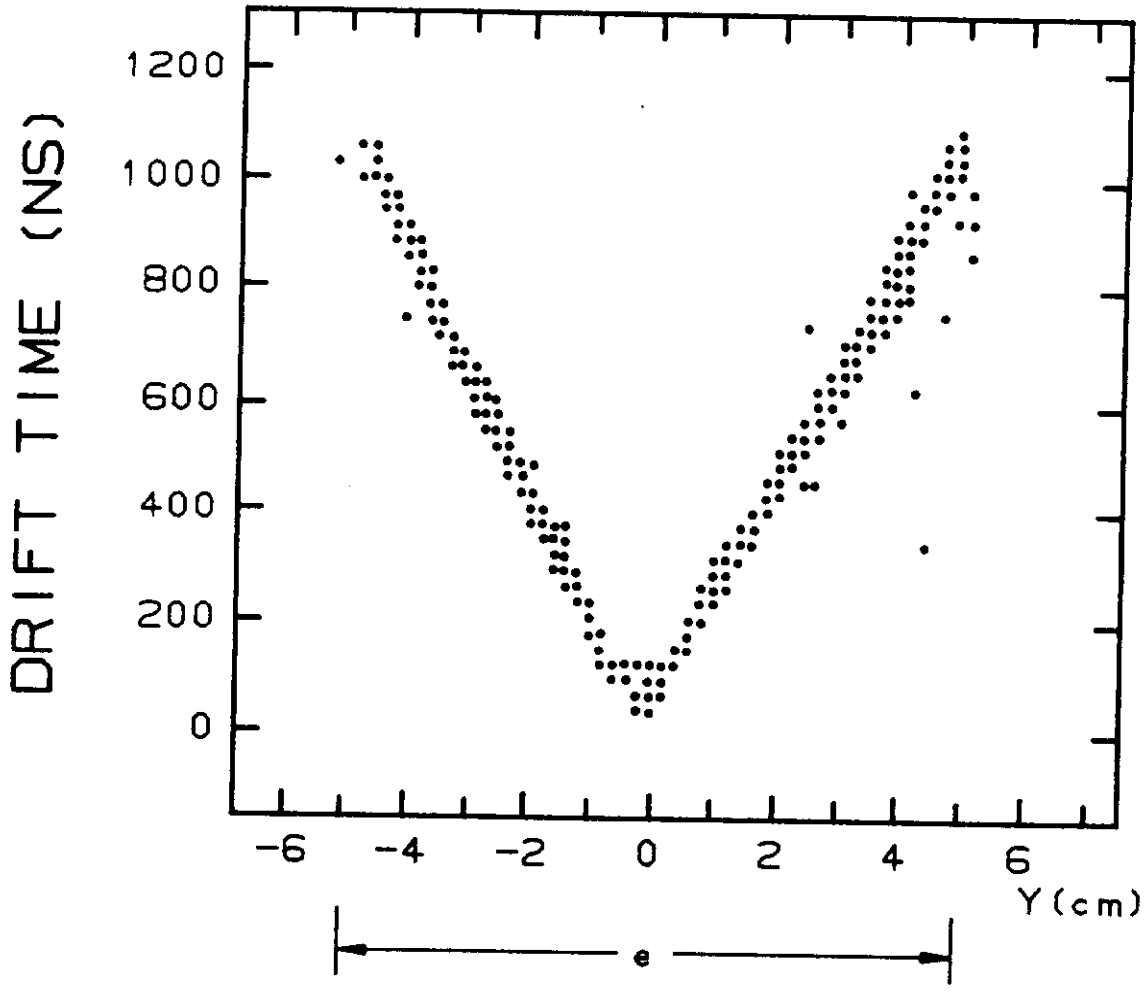

Fig. 2

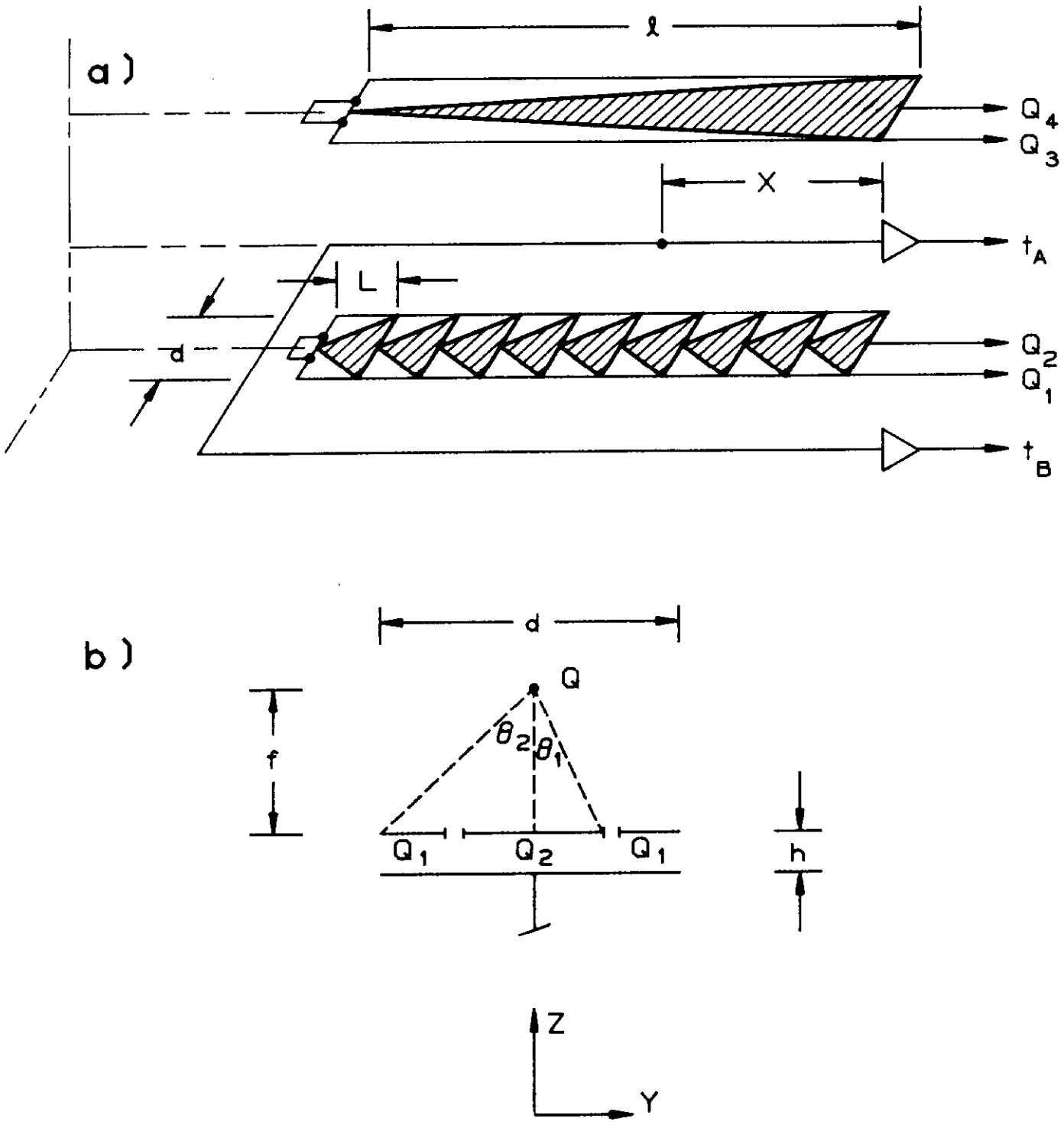

Fig. 3

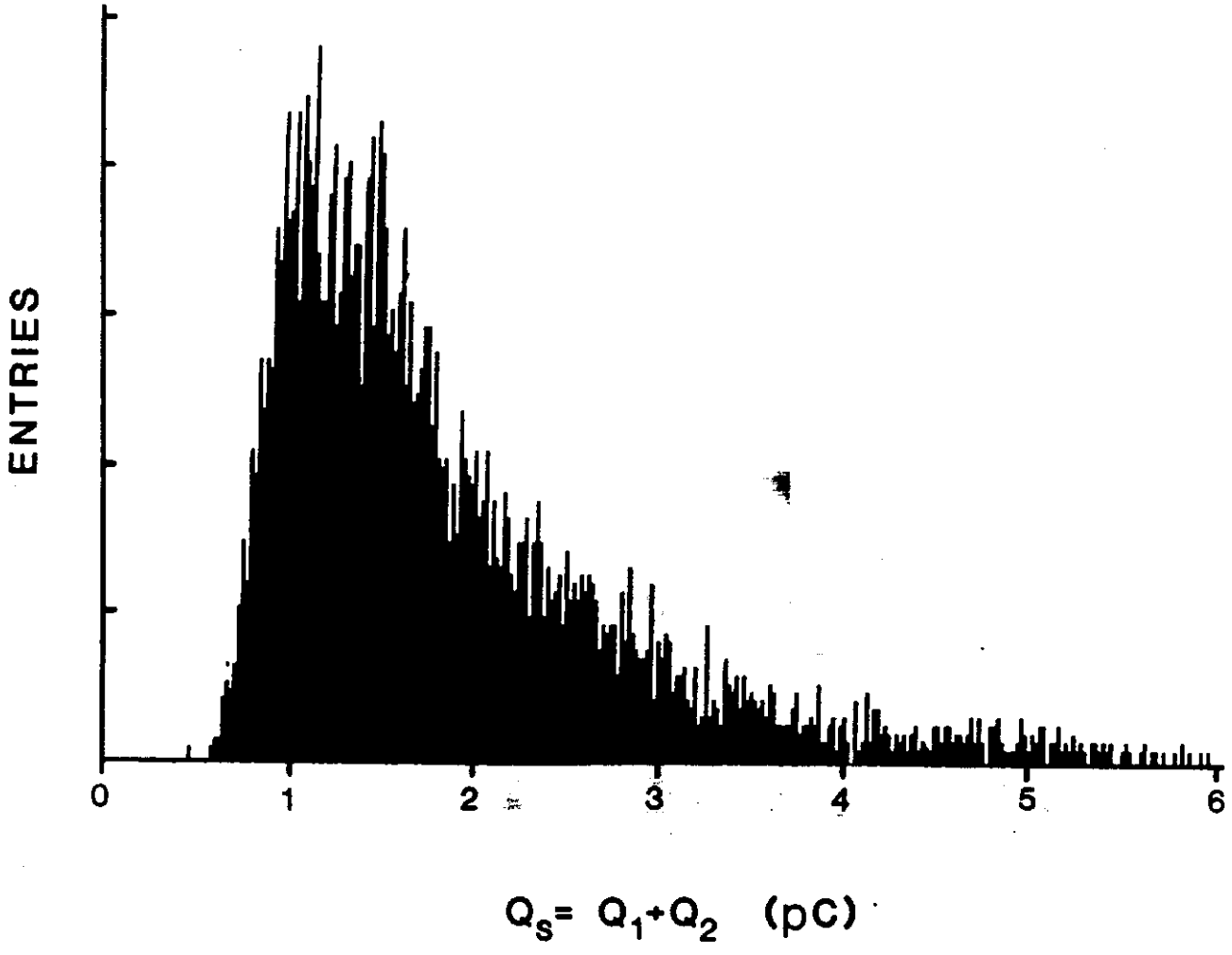

Fig. 4

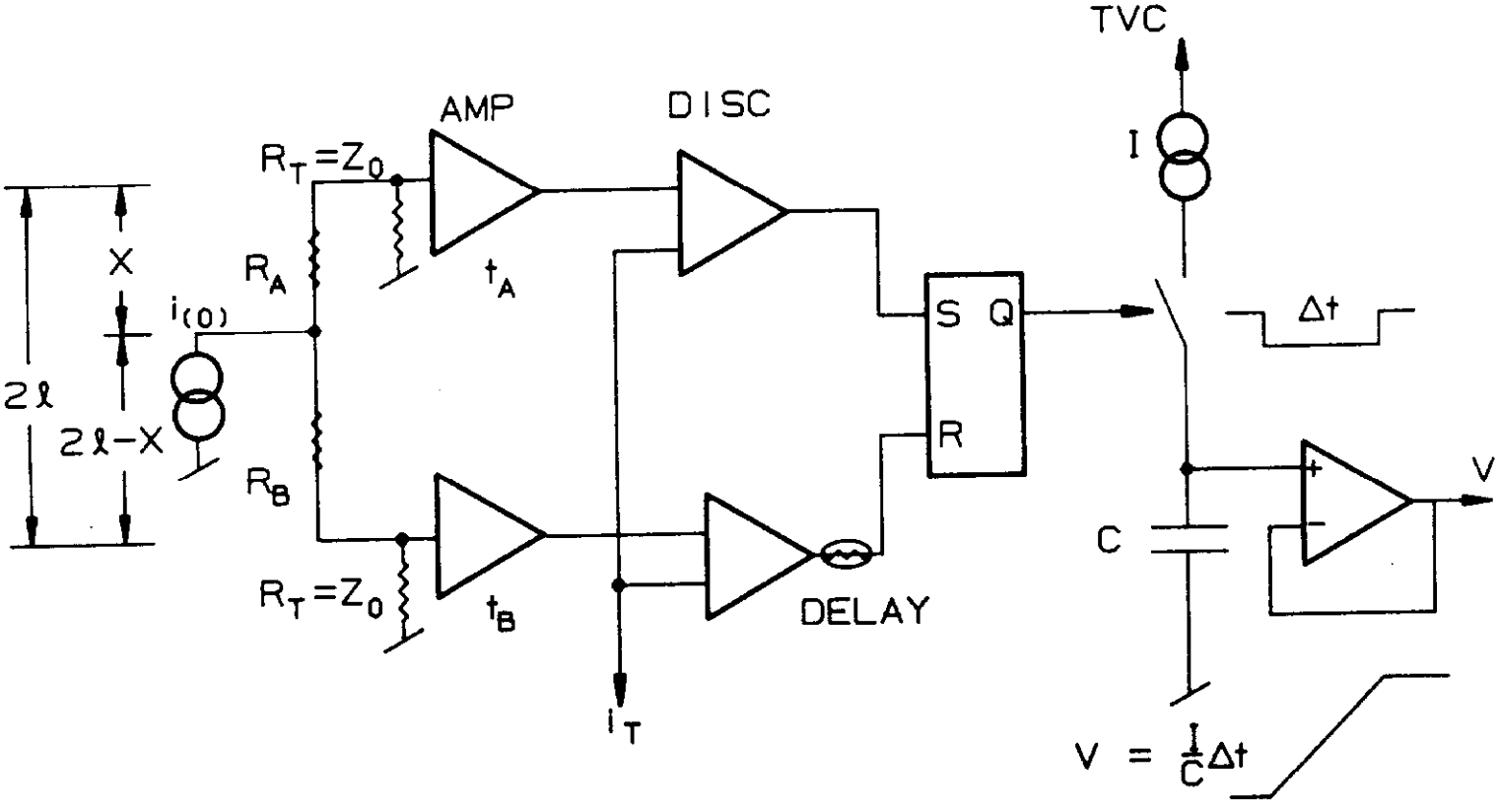
TVC
AMP
DISC
I
$R_T=Z_0$
X
R_A
t_A
$i_{(0)}$
S Q
Δt
2ℓ
2ℓ-X
R
V
R_B
C
$R_T=Z_0$
t_B
DELAY
i_T
$V = \frac{I}{C}\Delta t$

Fig. 5

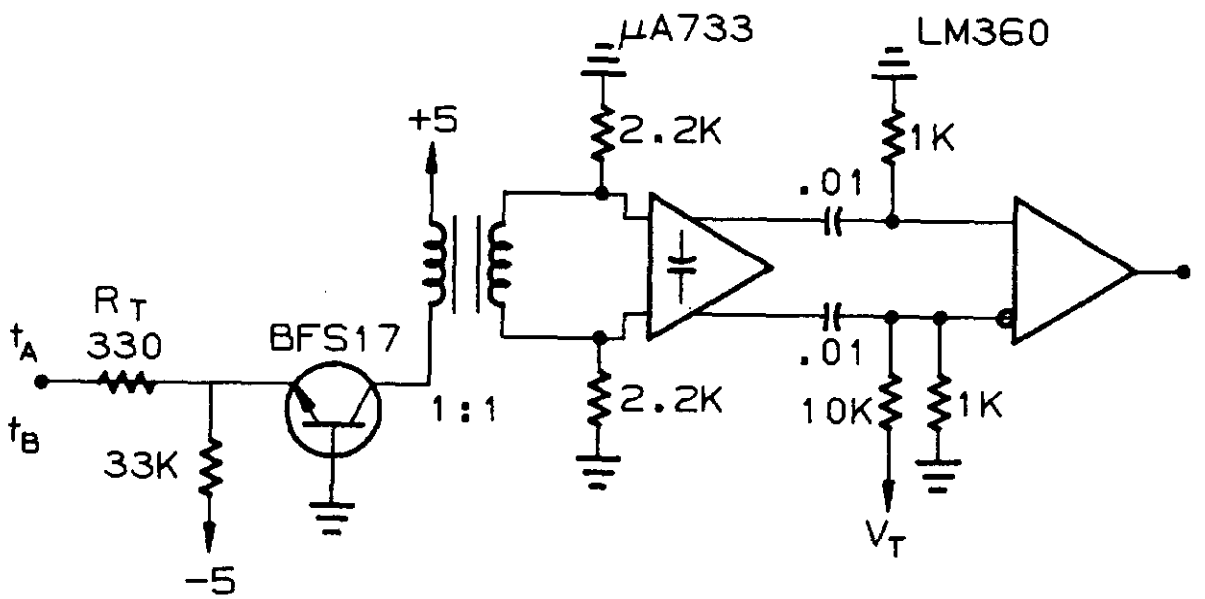
μA733
LM360
+5
2.2K
1K
.01
R_T
330
t_A
t_B
BFS17
1:1
.01
2.2K
10K
1K
33K
-5
V_T

Fig. 6

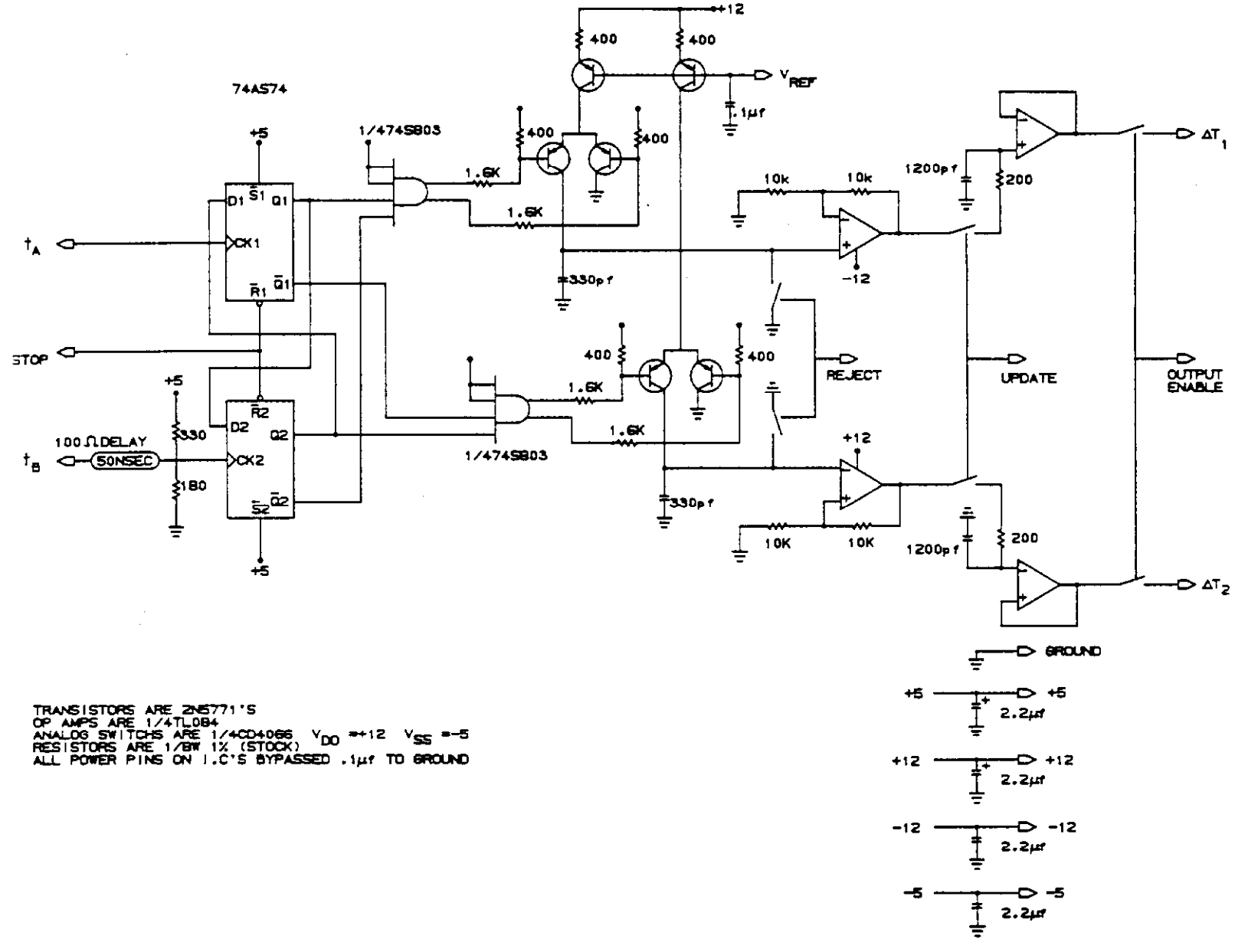

TRANSISTORS ARE 2N5771'S
OP AMPS ARE 1/4TL084
ANALOG SWITCHS ARE 1/4CD4066 V_{DD} =+12 V_{SS} =-5
RESISTORS ARE 1/8W 1% (STOCK)
ALL POWER PINS ON I.C'S BYPASSED .1µf TO GROUND

Fig. 7

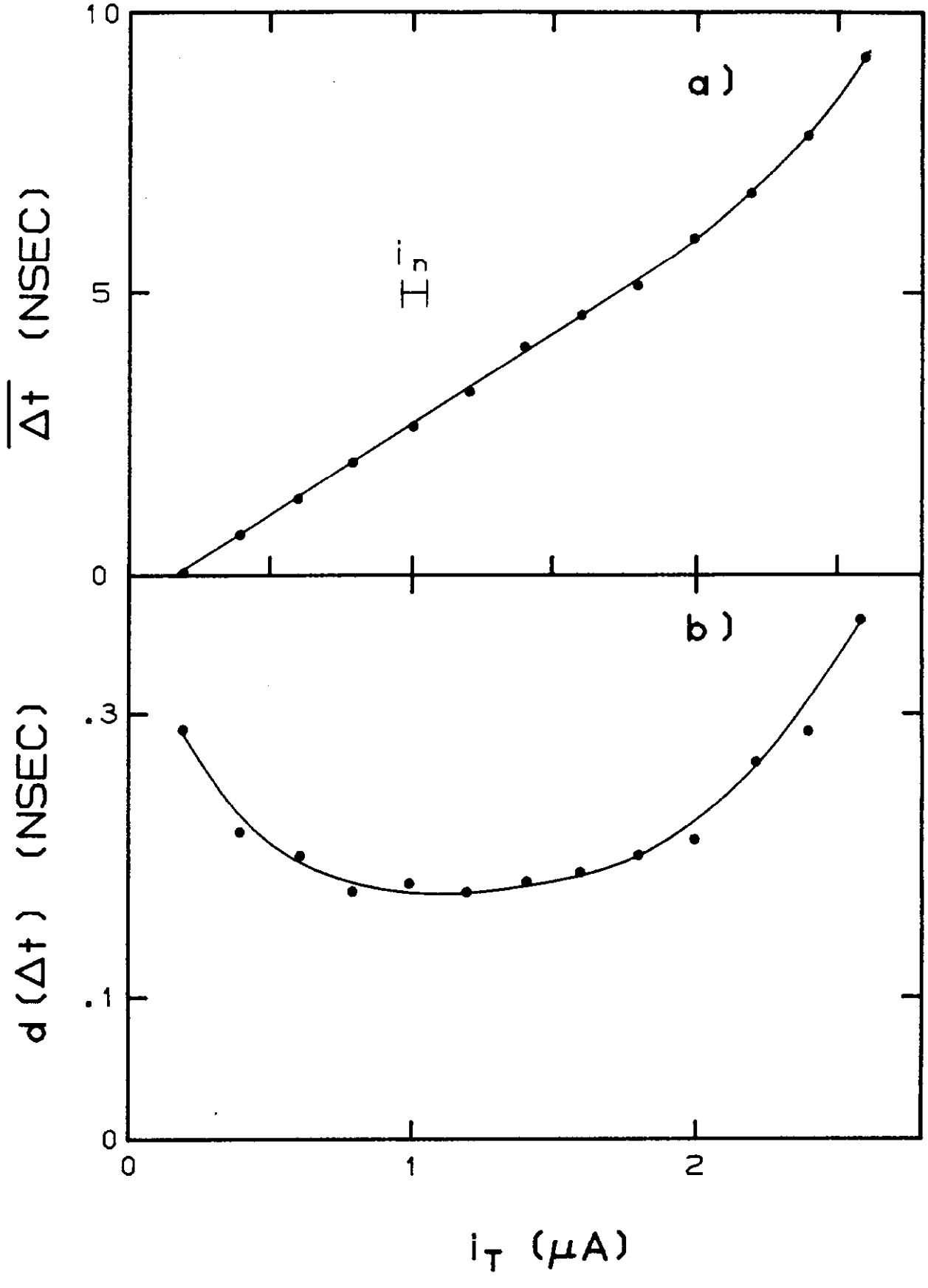

Fig. 8

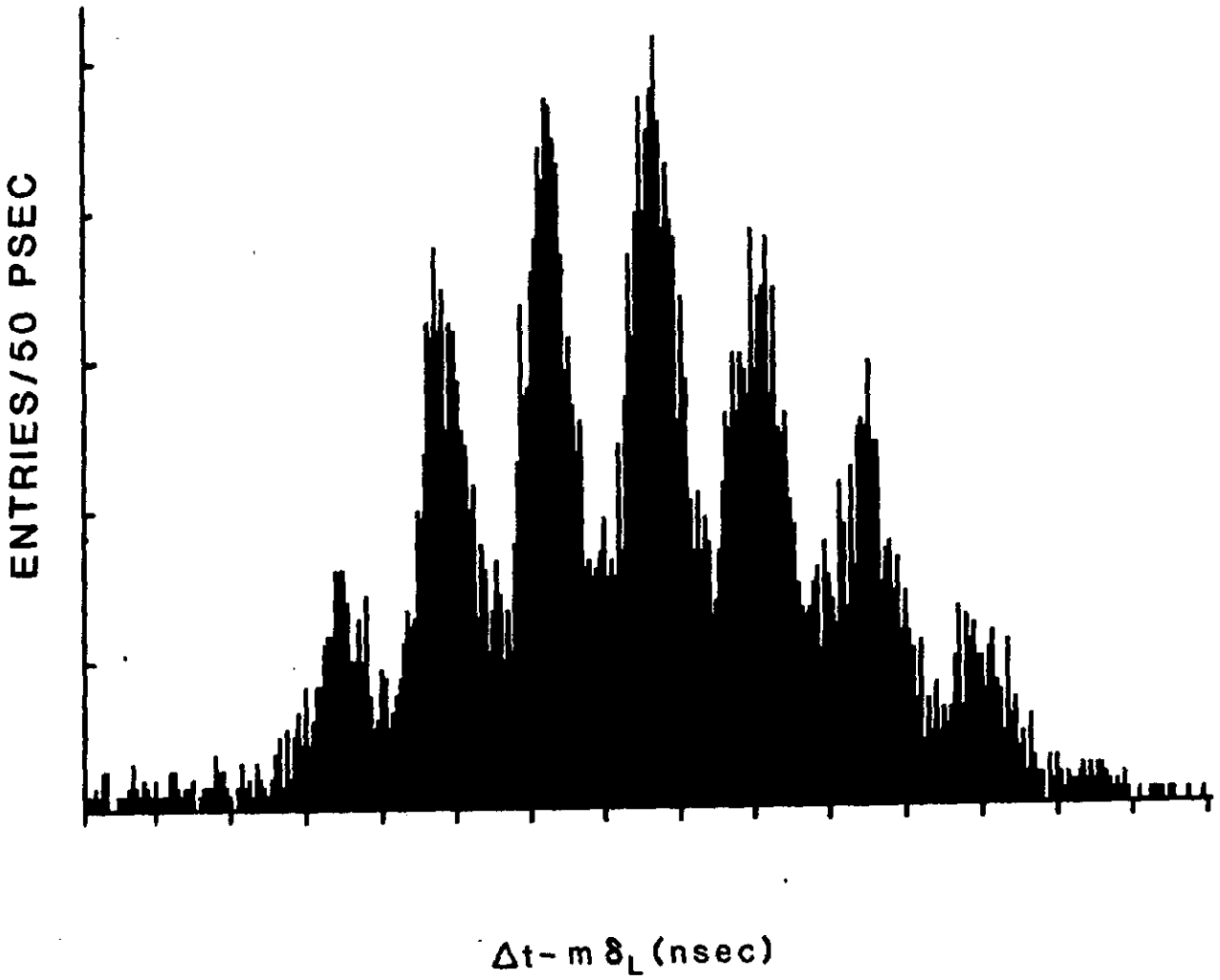

Fig. 9

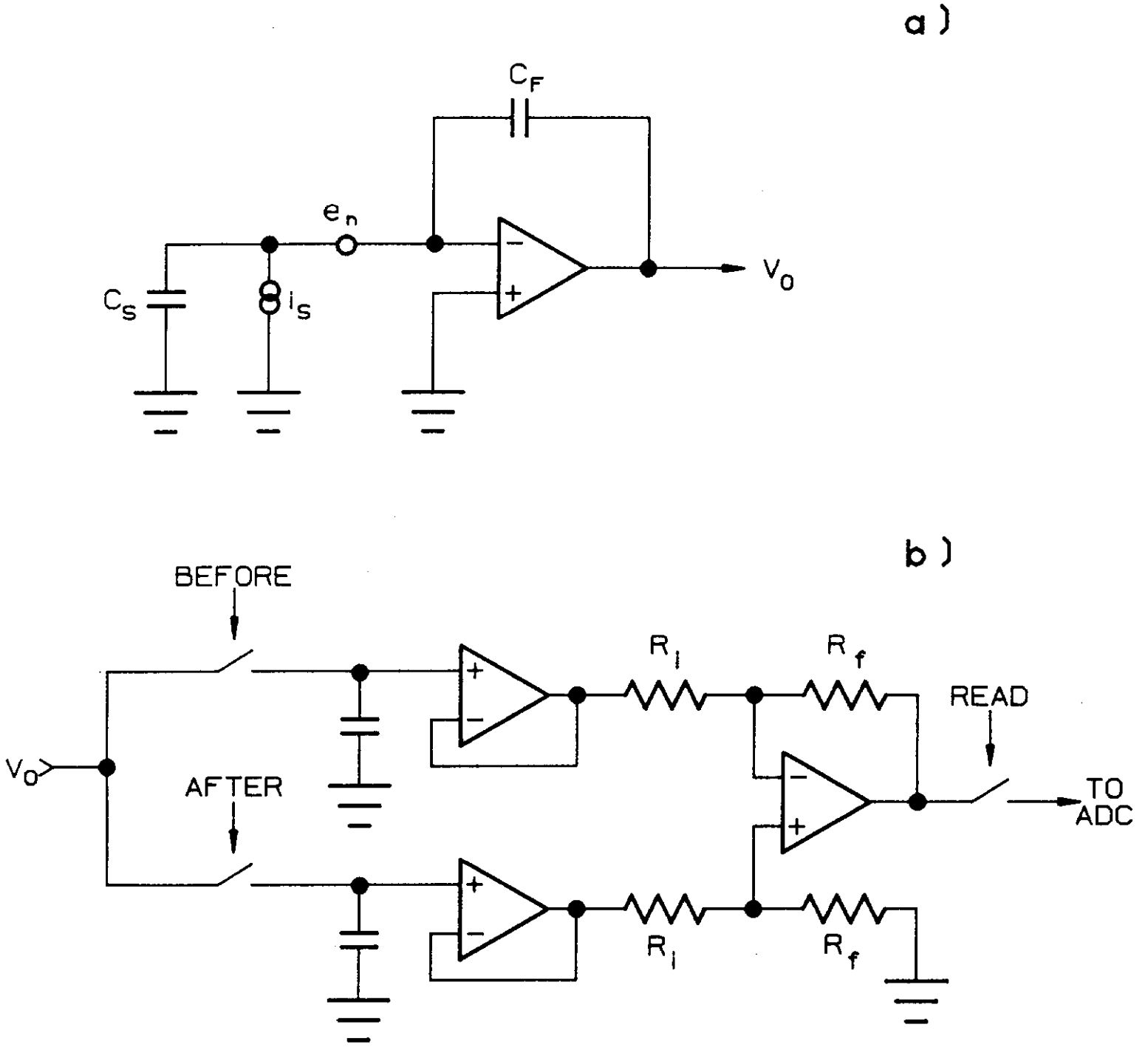

Fig. 10

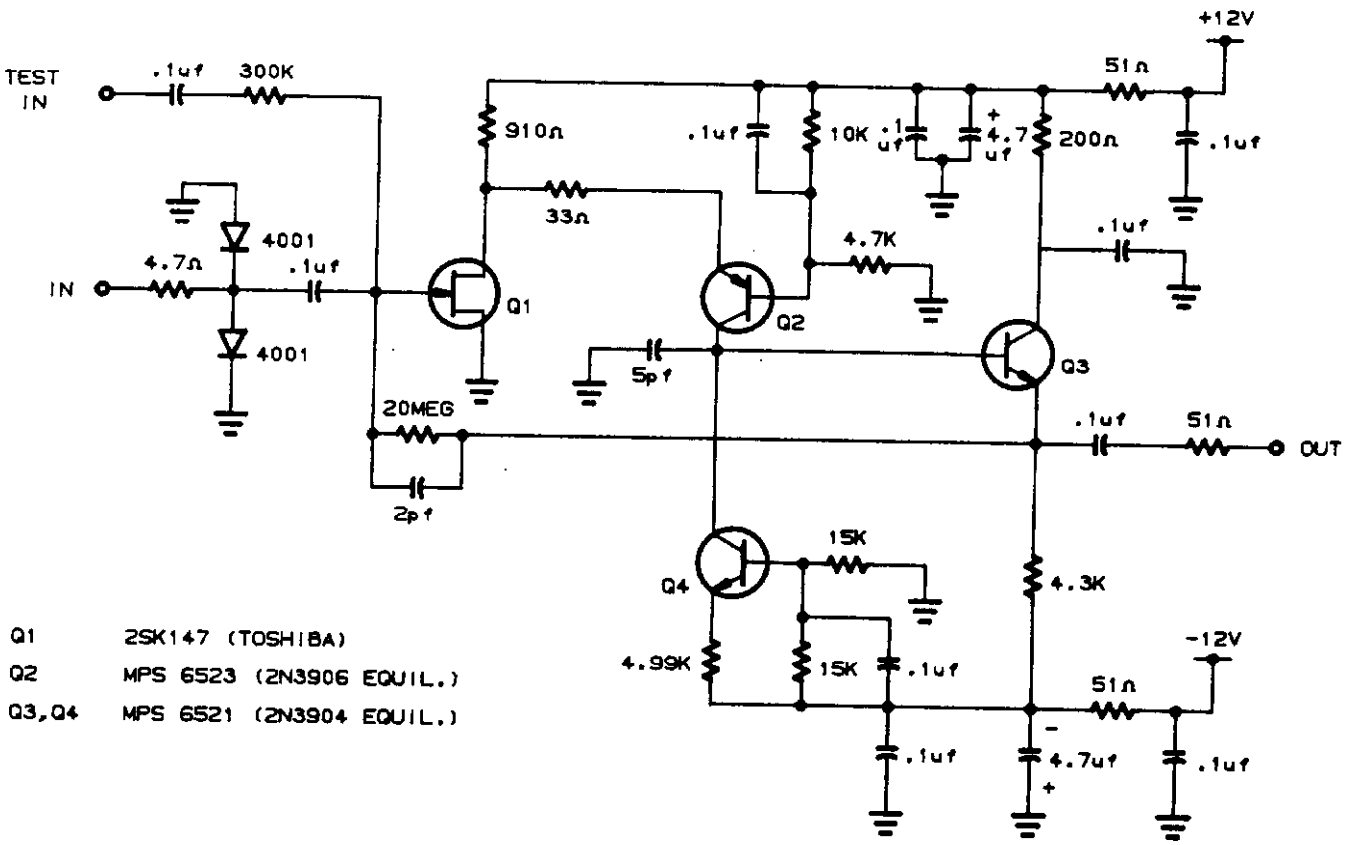
TEST IN
.1uf
300K
910Ω
33Ω
.1uf
10K
.1 uf
4.7 uf
200Ω
51Ω
+12V
.1uf
4001
4.7Ω
.1uf
IN
4001
Q1
Q2
4.7K
.1uf
5pf
Q3
20MEG
2pf
.1uf
51Ω
OUT
Q4
15K
4.3K
4.99K
15K
.1uf
-12V
51Ω
.1uf
4.7uf
.1uf
Q1 2SK147 (TOSHIBA)
Q2 MPS 6523 (2N3906 EQUIL.)
Q3,Q4 MPS 6521 (2N3904 EQUIL.)

Fig. 11

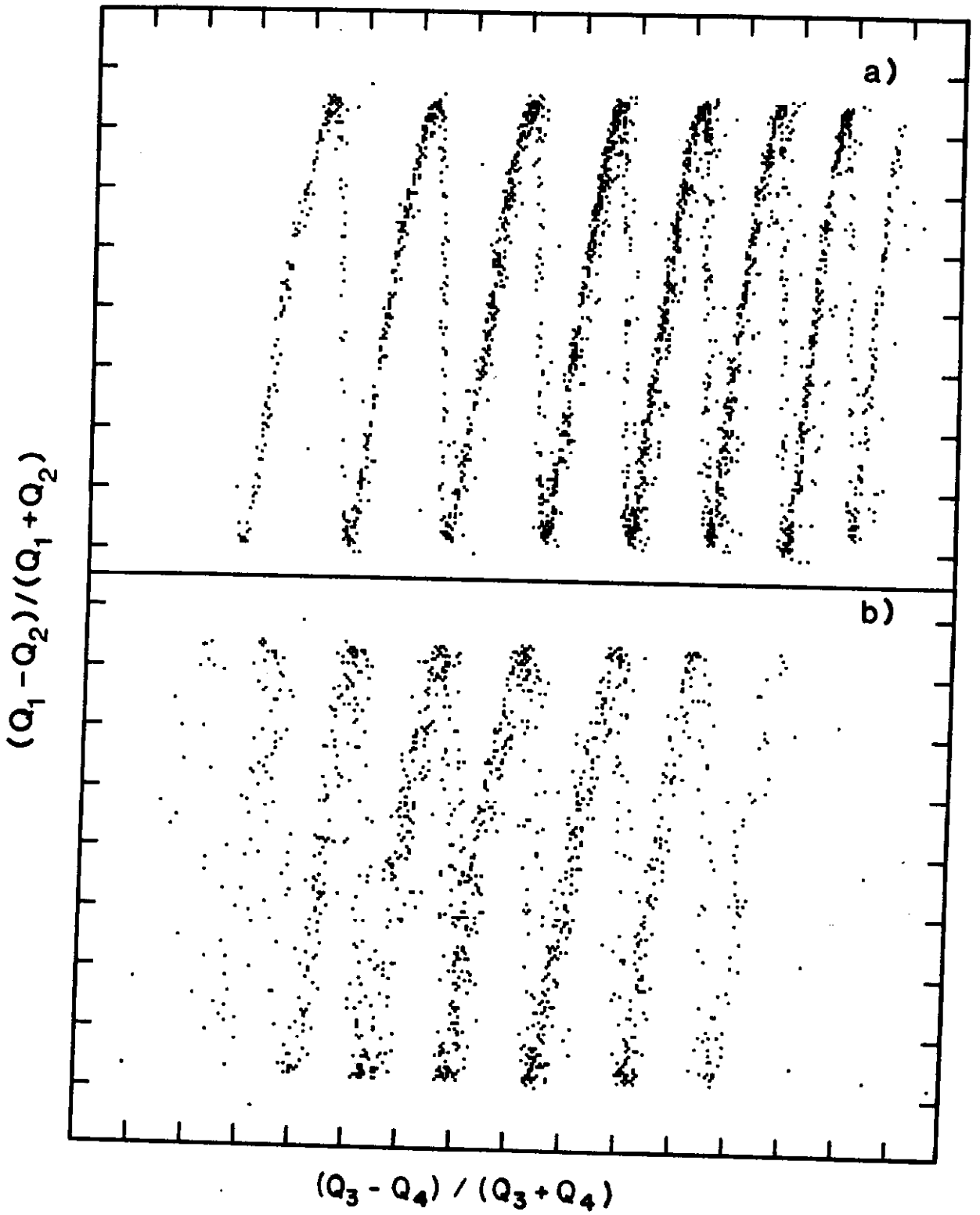

Fig. 12

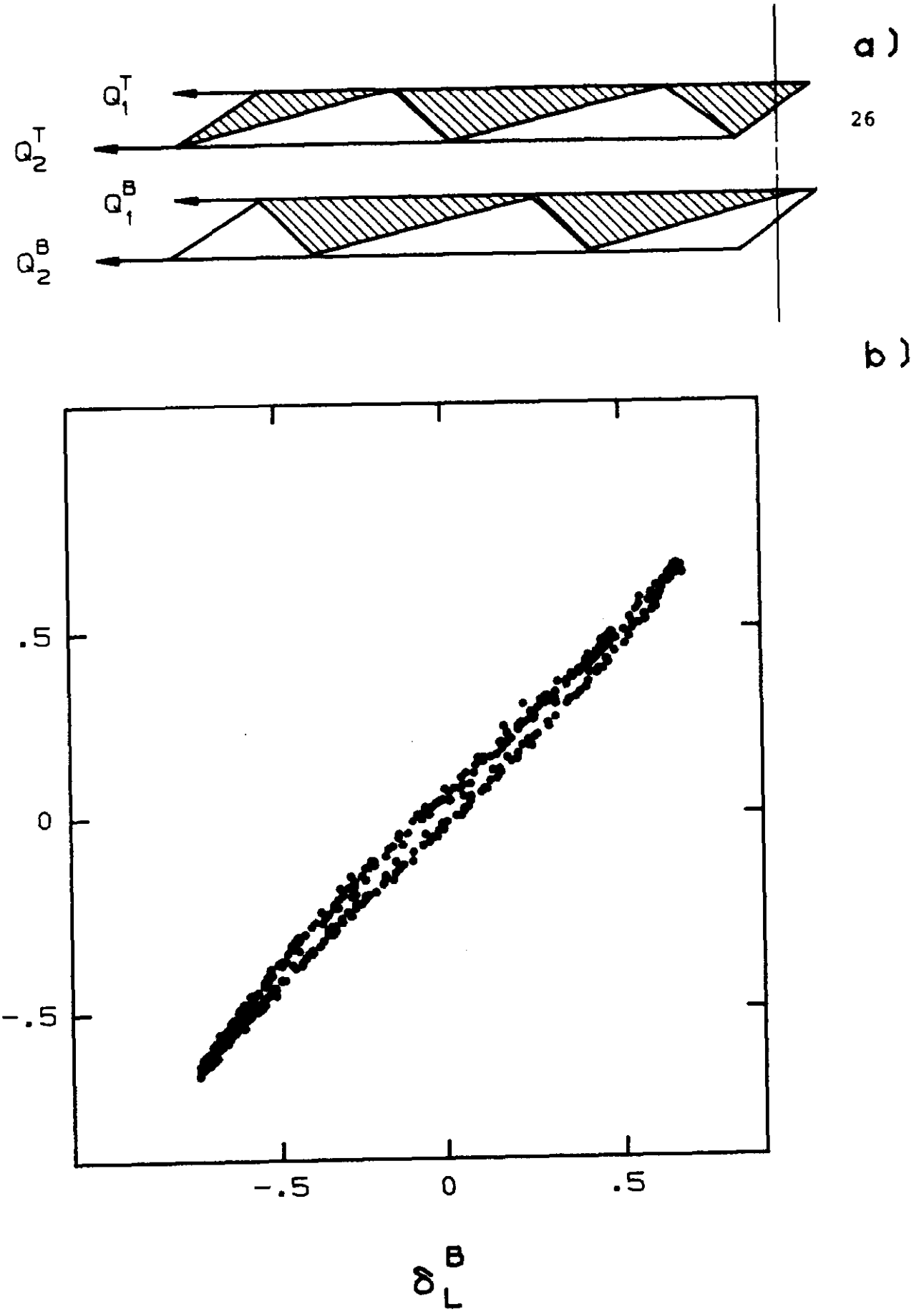

Fig. 13